Journal of Animal Environment

(E-ISSN 2717-1396, ISSN 2717-1388)

Original Research Paper

Effect of Low-Level Pulsed Laser-Assisted Processing of DNA-Modified Nano Raw Cellulose Obtained from Phoenix dactylifera Rachis on Achilles Tendon Healing in Rabbits.

Hanan Hakim Farhan, and Prof. Amir I. Towfik

Hanan Hakim; E-mail: vet.post24.21@qu.edu.iq , Amir Ibrahim ;E-mail amir.towfik@qu.edu.iq

ORCID iDs: https://orcid.org/0009-0006-1617-1578

Department of Surgery and Obstetrics / College of Veterinary Medicine / University of Al-Qadisiyah / Ad Diwaniyah–IRAQ

Abstract

Injuries of the Achilles tendon have a protracted healing process due to poor blood supply, low cell count, disorganised collagen orientation and reduced mechanical strength.This study examines the impact of low level pulsed laser assistance Phoenix dactylifera rachis raw nanocellulose on Achilles tendon healing in rabbits was evaluated in the presence of bacterial genomic DNA. Thirty senior New Zealand White rabbits were subjected to total Achilles tendon transection followed by modified Kessler repair and were split up into two equal groups at random.The control group wasn't treated just suturing whereas the experimental group was treated by 0.3 ML of DNA-modified raw nanocellulose Suspension , applied topically at the site of repair. The nanocellulose was characterised by FESEM, FTIR, XRD and UV-Vis spectroscopy. Healing was examined clinically, ultrasonographically, histopathologically and biomechanically at 0, 7, 14, 30 and 60 days postoperatively. FESEM confirmed the presence of nanoscale particles ranging from 25.81 to 41.28 nm. Compared to the control group, the treated group displayed greater clinical improvement, reduced inflammatory parameters, higher ultrasonographic tendon continuity, more structured collagen deposition, and improved mechanical strength. The results indicated that nanocellulose from the raw date palm rachis, obtained by low-level pulsed laser-assisted processing, could be a promising local biomaterial for experimental tendon rehabilitation.

Key Words: Raw Cellulose, Low intensity pulsed Laser , DNA, Achilles tendon, Ultrasound

.

Introduction

Achilles tendon injuries are tough to treat due to low cellularity, poor vascularity and sluggish extracellular matrix repair. Consequently, healing often results in disorganised scar tissue rather than a restoration of the usual pyramidal structure of collagen fibres, resulting in decreased mechanical qualities, adhesions, and an increased risk of recurrence . Nanocellulose is a promising biomaterial for tendon regeneration. It has excellent tensile strength, nanofibrous structure and water retention capacity. It can also modulate the porosity and is biocompatible. These qualities enable nanocellulose to replicate the key features of the extracellular matrix of the tendon, facilitate fibroblast adhesion and proliferation, and enhance collagen deposition and tissue remodelling . Moreover, this new regenerative biomaterial should successfully help to modulate the inflammatory response, direct the alignment of collagen fibres and induce the biomechanical maturation of the restored tissue . Thus, the application of nanocellulose could be an efficient regenerative therapeutic approach for

***Corresponding Author:**

Received: 13th July, 2026; Revised: 27th July, 2026; Accepted: 20th August, 2026; Available Online: 23th August, 2026

(DOI): 10.70102/AEJ.2026.18.4s.27

the healing of the Achilles tendon in experimental animal models such as rabbits.[1–3]

2. Materials and Methods

2.1 Approval of ethics

The University of Al-Qadisiyah, Iraq's College of Veterinary Medicine Research Ethics Committee approved all animal procedures (Ref. No. 1012, 9 March 2026). "Every effort was made to minimise pain and suffering.

2.2. Preparation of cellulose-rich raw material from date palm rachis

The rachis of date palm, Phoenix dactylifera L. was harvested locally in the area, cleaned, cut into small pieces, sun dried to a constant weight and milled in electric mill. The resulting powder was sieved to get the particle size more homogenous and to get the solvent to penetrate the powder more. The sieved powder was used for the extraction. 20 g of the powder thus sieved was refluxed with 500 mL of 99% ethanol in a cellulose extraction thimble (in a Soxhlet apparatus) to remove ethanol soluble chemicals such as waxes, oils, pigments etc. from the powder leaving the fibrous part of the lignocellulosic structure intact. No alkaline treatment or bleaching or acid hydrolysis was carried out, and the resulting product was not chemically treated cellulose or cellulose nanocrystals but rather a cellulose-rich raw material of lignocellulosic material. This chemically conservative approach wasThe cellulose associated lignocellulosic was selected because it contained less strong chemicals. The components can be preserved as a minimally processed natural biomaterial to use in experiments involving tendon. repair [4–8]

Figure (**1**): palm rachis raw cellulose before and after extraction.

2.3 Aqueous extract of seeds of Albizia lebbeck

The seeds of Albizia lebbeck were washed, sun dried, ground to powder and sieved. The powdered seeds (50 g) were mixed with 100 mL of distilled water and cooked while stirring constantly. After that, the extract was brought to room temperature. filtered ,stored with sterile containers and frozen until required. The extract was employed as a natural stabilizing phase because it contains phytochemical and water soluble polysaccharide components which might be responsible for capping and the colloidal stability of A. lebbeck [9–10].

2.4 Genomic DNA of bacteria

Bacterial genomic DNA Bacterial genomic DNA of Escherichia coli was provided by Wahaj Al-Dana Company, Baghdad, Iraq, and used as a stabilizing biopolymer in the synthesis of nanocellulose. The concentration and purity of the DNA were measured by using a NanoDrop UV-visible spectrophotometer before use. The concentration was 937.2 ng/µL with an A260/A280 ratio of 1.8 with good purity. DNA integrity was confirmed by agarose gel electrophoresis. The DNA was used because its negatively charged phosphate backbone may enhance electrostatic stabilization and reduce particle aggregation [11–15].

2.5 Preparation of nanocellulose aided by low-level pulsed laser

A chemically conservative physical technique was used to manufacture raw nanocellulose from a cellulose-rich lignocellulosic fraction of *Phoenix dactylifera* rachis. The starting material was viewed as a raw cellulose-rich fraction, not refined cellulose nanocrystals, because alkaline delignification, bleaching and acid hydrolysis were avoided [4–8,16]. Each preparation consisted of 2 g of crude cellulose-rich material, dispersed in 1ML of deionize water, then 0.5 mL of aqueous Albizia lebbeck seed extract as a natural stabilizing phase [9–10]. The suspension was placed in a clear glass tube and irradiated with a low level pulsed diode

laser at 660 nm, 250 mW, 146 Hz, and 8 J/cm² for 20 s. The exposure geometry was kept stable by pressing the laser probe into touch with the external wall of the tube. Total supplied energy was 5 J with an estimated irradiation area of 0.625 cm², an approximate beam width of 8.9 mm and a power density of 0.4 W/cm². For irradiation, pure *Escherichia coli* genomic DNA was added dropwise to a final volume of 0.5 mL at a rate of approximately 25 µL/s with a sterile micropipette.

The laser was utilized as a physical size-reduction assist, rather than a chemical synthesis instrument or therapeutic laser treatment. Localized photothermal and photomechanical agitation, pressure fluctuation, and microstreaming can be induced in the hydrated solution by repeated pulsed irradiation, which may weaken cellulose-rich clumps and encourage their dispersion into nanoscale structures [5,7–8,17]. As no metal salt was introduced, the mechanism was not understood as metal-ion reduction or metallic nanoparticle production. The stabilization was attributed to the non-covalent interactions with the A. lebbeck extract and to the negatively charged phosphate backbone of bacterial DNA that might increase the electrostatic repulsion and decrease the particles re-aggregation [9–10,13–15]. Since we did not undertake direct surface binding investigation, we describe the result as raw nanocellulose synthesized in the presence of bacterial genomic DNA, and not DNA-coated nanocellulose.

The solution was freshly made under clean aseptic handling utilizing sterile glassware and sterile disposable tips prior to topical application. It did not promise to be terminally sterile or endotoxin free. The absence of 0.22 µm filtration, UV sterilization, validation of sterility, quantification of endotoxin, zeta potential, particle size distribution and PDI were recognized as a restriction and suggested to be optimized in future [7,13–15,18,22]. NanoDrop was defined as a UV-visible spectrophotometer and DNA integrity was measured by agarose gel electrophoresis [11–12].

Figure (2): It explains the method of converting extracts into nano using a low level pulsed laser (omega laser system).

2.6 Animals, surgery and care

Rabbits were anesthetized with a ketamine–xylazine combination, according to the approved protocol [19]. The hind limb was shaved and prepared aseptically. A longitudinal skin incision of about 2.5 cm was made over the achilles tendon, which was carefully separated from the surrounding tissues. A full transverse tenotomy approximately 1 cm proximal to the hock/calcaneal insertion was performed to standardize the Achilles tendon damage model [20–21]. The ends of the tendons were repaired using modified Kessler tenorrhaphy technique with absorbable monofilament polydioxanone suture and the skin was closed with polypropylene sutures. After surgery the operated limb was clothed and supported with a compression bandage.

Animals were treated according to group after tendon repair and before skin closure. In G1 (control group), 0.3 mL of phosphate-buffered saline was locally administered at the site of repair. 0.3 mL of fresh DNA-modified raw nanocellulose suspension was administered topically on the reconstructed tendon in G2. The idea was that this local application would allow direct interaction of the nanocellulose suspension with the early tendon healing interface. Nanocellulose based biomaterials have been described as a supporting interface for tissue restoration due to its high surface area, hydrophilicity and biocompatible structure [7,22–23].

2.7 Ratings and statistics

Clinical, ultrasonographic, histological and biomechanical evaluations were performed on days 0, 7, 14, 30 and 60. Clinical signs were reported as the proportion of animals presenting each indication. The phrase clicking was eliminated and replaced by adhesion tendency or tendon gliding . Mechanical measurements are load/tensile resistance in Newtons (N) and not MPa or N/mm2 Data are given as mean +/- SE and analysed by post-hoc comparison using ANOVA. P less than 0.05 was regarded as statistically significant.

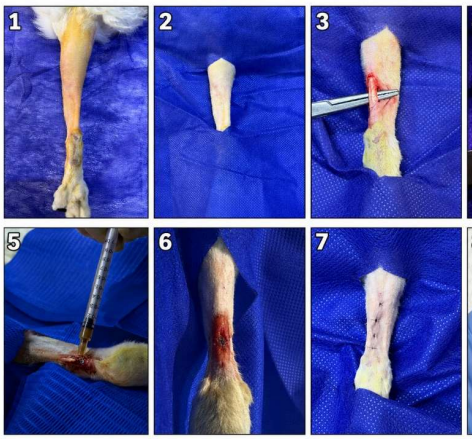

Fig(2);-Surgical induction and repair of complete rupture of the Achilles tendon in a rabbit. (1) Limb preparation. Identification of the surgery field and the tendons. (3)Tendon exposure. (4) Complete transverse tenotomy. (5) Application of nanocellulose topically and tendon repair. (6) Modified Kessler repair. (7) Skin closure. (8) Dressing and compression bandage after surgery.

3. Results

3.1. Characterization of nanocellulose

The FESEM revealed the presence of dense spherical to subspherical nanoparticles in the range of 25.81 to 41.28 nm which are grouped together in overlapping nanoclusters. The XRD showed a strong diffraction peak at around 2theta of 28 degrees with a broad background, which is indicative of a semi crystalline material; this may be due to the high surface energy and hydrogen bonding interactions. The UV-Vis spectroscopy revealed the absorption peak at 273 nm and absorbance of 0.469. FTIR showed bands at 3400 cm-1, 2922-2854 cm-1, 1653 cm-1 and 1516 cm-1 which confirmed the presence of essential functional groups of lignocellulosic structure.

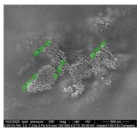

A. ESEM showing nanoscale spherical to subspherical particles.

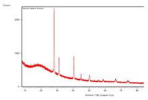

B. XRD pattern showing semi-crystalline behavior.

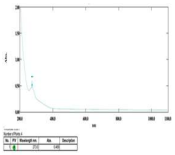

C. UV-Vis absorption peak at 273 nm.

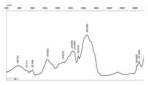

D. FTIR spectrum showing preserved lignocellulosic bands.

3.6 Analysis of biomechanics

A biomechanical investigation was performed to measure the experimental tensile resistance of the repaired Achilles tendon by a mechanical spring force gauge.

First readings were in gram-force (gf) and were converted to Newtons (N) using the equation:

Force (N) = Force (gf) * 0.00980665

The same factor was applied to translate means and standard errors . The recorded data were experimental tensile resistance/load bearing capacity and were not normalized, hence findings were not reported in MPa or N/mm² as tendon cross-sectional area was not measured. Table 1. Tensile resistance of repaired Achilles tendon for rabbit (experimental. Values were

originally in gram-force and converted to Newtons . Data are expressed as mean±S.E. (N).

Table 1. Experimental tensile resistance of repaired Achilles tendon in rabbits expressed as mean ± SE (N).

roup	ay 0	ay 7	ay 14	ay 30	ay 60
1 Contr ol	.93 ± 0.03	.08 ± 0.05	.52 ± 0.03	.73 ± 0.04	.93 ± 0.03
2 Nanoc ellulo se	.96 ± 0.02	.24 ± 0.02	.13 ± 0.04	.42 ± 0.03	.45 ± 0.00

All groups showed equal tensile resistance values on day 0, confirming that the immediate postoperative baseline conditions were identical after standardized transection of the Achilles tendon and modified Kessler repair. Hence, the Day 0 data were taken as the baseline mechanical parameters prior to the commencement of any healing effect associated to the treatment. Upon follow-up, increasing increase in tensile resistance was observed in both groups, indicating ongoing tendon healing and collagen remodeling. However, the nanocellulose treated group had higher values than the control group, in particular at Days 14, 30 and 60. This finding reveals that topical application of raw nanocellulose increased the functional load bearing capacity of the regenerated tendon and promoted collagen maturation. These biomechanical results were consistent with ultrasonographic and histological results that demonstrated higher tendon continuity, better fibrillar organization, and more organized collagen deposition in the treated group.

3.6 Ultrasonographic findings

At Day 0, both groups showed disturbed fibrillar pattern, local thickening, irregular boundaries and hypoechoic-to-mixed repair areas consistent with immediate post-surgical changes. At 7 days, G1 showed persistent mixed echogenicity, disrupted fibrillar architecture, tendon thickening and residual edema, whereas G2 showed early repair tissue and more restricted surrounding fluid. At 14 days, G1 still showed heterogeneity and poor fiber continuity, while G2 showed gradual narrowing of the hypoechoic gap and better margin regularity. At 30 days, G1 showed thickened heterogeneous repair tissue with residual hypoechoic foci, whereas G2 showed more homogeneous echogenicity and clearer fiber convergence. At 60 days, G2 showed clearer fibrillar pattern, increased echogenicity and better tendon continuity.

Figure Plate 3. Ultrasonographic healing at Day 0, Day 7 and Day 14

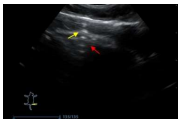

A. G1 Day 0: Longitudinal ultrasound image of the reconstructed Achilles tendon immediately after surgery, showing standardized acute post-surgical baseline changes with a disturbed fibrillar pattern, local thickening, irregular boundaries, and a hypoechoic-to-mixed repair area with mild edema. Yellow arrows indicate echogenic suture/repair material, while the red arrow indicates the hypoechoic edematous repair region.

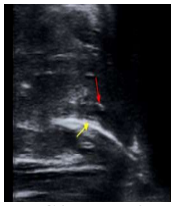

B. G2 Day 0: Longitudinal ultrasound image of the reconstructed Achilles tendon immediately after surgery, showing comparable acute post-surgical baseline changes with disturbed fiber structure, local thickening, irregular tendon borders, and a hypoechoic-to-mixed repair area with simple fluid/mild early edema. Yellow arrows indicate hyperechoic suture-related foci, while the red arrow indicates the hypoechoic gap or early edema. No treatment effect was interpreted at this baseline time point.

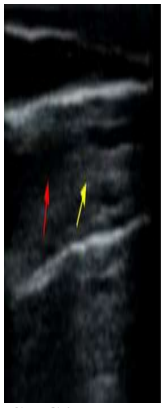

C. G1 Day 7: Longitudinal ultrasound of the repaired Achilles tendon. Yellow arrows indicate a mixed-echogenic repair zone with disrupted fibrillar architecture, while the red arrow indicates a small adjacent hypoechoic area consistent with residual edema or peritendinous fluid. Findings suggest persistence of the early inflammatory phase, with tendon thickening, heterogeneity, and minimal residual fluid.

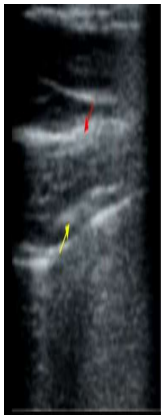

D. G2 Day 7: Longitudinal ultrasound image of the repaired Achilles tendon showing continuation of the early inflammatory phase with a mixed-echoic repair area. The incision site began to fill with repair tissue more clearly than at baseline (yellow arrows). Surrounding fluid was more restricted, and the peritendinous sheath was more clearly defined than in G1. Significant local thickening remained, with slight improvement in border regularity compared with Day 0 (red arrows).

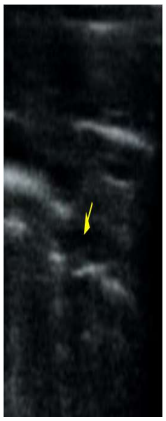

E. G1 Day 14: Longitudinal ultrasound image of the Achilles tendon showing heterogeneous tendon tissue, reduced echogenicity at the injury site, poor regularity, and incomplete fiber continuity, indicating persistent edema and incomplete healing.

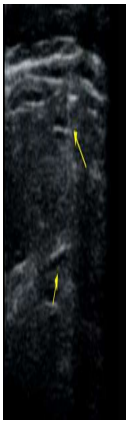

G2 Day 14: Longitudinal ultrasound image of the Achilles tendon showing early repair tissue at the suture site, with continued disturbance of the fibrillar pattern compared with baseline and week 1. Echogenicity was low-to-mixed, the tendon remained thicker than usual, and margins had begun to regularize but were not fully formed. No large fluid pockets were present; if visible, they were small and peripheral. Shiny foci likely represented suture/knot material, with mild edema indicating inflammation. Compared with baseline and the previous week, there was more pronounced convergence and gradual narrowing of the hypoechoic gap.

Figure Plate 4. Ultrasonographic healing at Day 30 and Day 60

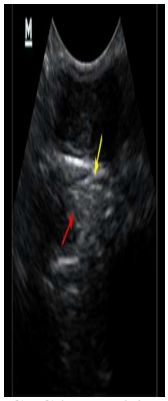

G. G1 Day 30: Longitudinal ultrasound image of the Achilles tendon showing a thickened, heterogeneously hyperechoic repair area (yellow arrows) with residual hypoechoic foci and irregularity within the tendon (red arrow). Findings indicate improvement compared with early stages, although persistent thickening and fibrillar disorganization suggest incomplete remodeling.

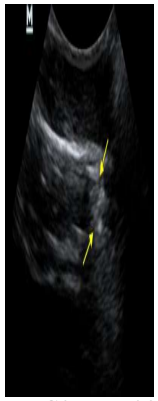

H. G2 Day 30: Longitudinal ultrasound image of the Achilles tendon showing relative improvement in the regularity of the fibrillar pattern with increased echogenicity compared with the control group, indicating progress in healing. The tissue appeared more homogeneous, with clearer fiber convergence (yellow arrows), reflecting the effect of cellulose in accelerating tissue remodeling.

I. G1 Day 60: Longitudinal ultrasound image of the Achilles tendon showing increased echogenicity and improved fiber continuity across the scar (yellow arrows), with residual focal heterogeneity at the repair site (red arrow). Findings indicate advanced scar maturation, improved tendon margins and fibrillar organization, and absence of visible peritendinous fluid despite limited focal irregularity.

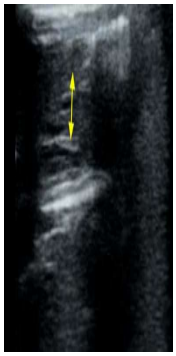

J. G2 Day 60: Longitudinal ultrasound image of the Achilles tendon showing a clear, regular fibrillar pattern with increased echogenicity, indicating improved collagen fiber reorganization. Good tissue homogeneity was also observed and appeared better than in the control group.

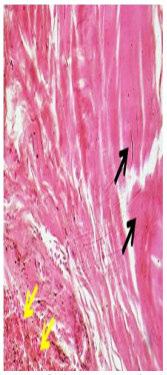

A. G1 Day 0: Histological section of the Achilles tendon showing standardized acute post-surgical baseline changes, including extensive tendon fiber disruption (black arrows), hemorrhage and fibrinous clot formation at the injury site (yellow arrows), with early inflammatory cell migration. No established fibroblast proliferation or healing tissue formation was interpreted at this immediate time point. H&E stain, 40X.

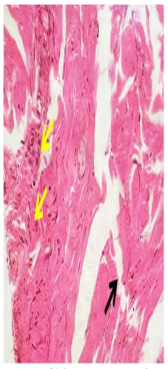

B. G2 Day 0: Histological section of the Achilles tendon showing comparable acute post-surgical baseline changes, including tendon fiber disruption, hemorrhage/fibrinous material, and mild early inflammatory infiltration. No established fibroblast proliferation or treatment-related healing response was interpreted at this immediate time point. H&E stain, 40X.

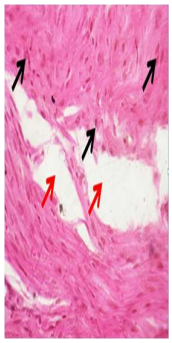

C. G1 Day 7: Histological section of the Achilles tendon showing gradual but limited early recovery. Spaces between collagen fibers are observed (red arrows). At this period, the tendon repair region displayed a moderately severe inflammatory reaction, with granulation tissue and early fibroblast proliferation (black arrows). H&E stain, 40X.

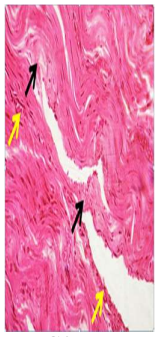

D. G2 Day 7: Histological section of the Achilles tendon showing a better healing response, with noticeable reduction in inflammation and enhanced cellular organization compared with the suture-only group. A slight-to-moderate inflammatory response was observed at the repair site (yellow arrows), but it was less pronounced than in the control group. Early collagen deposition was apparent as delicate, loosely connected fibers (black arrows) within emerging granulation tissue, and fibroblast proliferation was more noticeable. H&E stain, 40X.

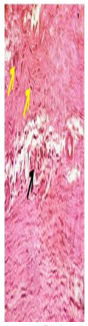

E. G1 Day 14: Histological section of the Achilles tendon showing enhanced collagen deposition, while the repair area still displayed a moderately significant inflammatory response. Granulation cells and early fibroblast proliferation were present (black arrows). H&E stain, 40X.

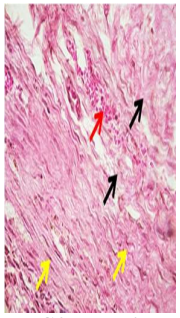

F. G2 Day 14: Histological section of the Achilles tendon showing markedly increased fibroblast proliferation and extracellular matrix synthesis (black arrows), with decreased inflammatory infiltrate. Collagen fibers appeared denser and started to partially align along the longitudinal tendon axis as collagen accumulation became more noticeable (yellow arrows). Compared with previous time points, the tissue showed better organization, and blood supply began to improve in this group (red arrow). H&E stain, 40X.

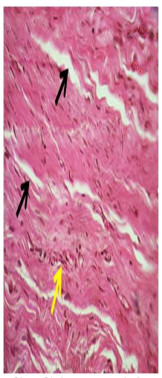

G. G1 Day 30: Histological section of the Achilles tendon showing numerous spaces between collagen fibers (black arrows). Collagen accumulation became more noticeable, and inflammation had decreased significantly; however, collagen fibers remained haphazardly organized and disordered, resulting in scar-like tissue rather than a normal tendon-like architecture (yellow arrows). H&E stain, 40X.

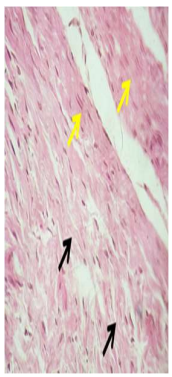

H. G2 Day 30: Histological section of the Achilles tendon showing mild collagen development and better collagen bundle organization in the healing tissue (black arrows). Fibers resembled the framework of early tendon tissue, being more evenly spaced and partially parallel (yellow arrows). Although vascularization was still present, it had started to decline, suggesting progression of tissue remodeling. Cellular density was also reduced compared with earlier phases. H&E stain, 40X.

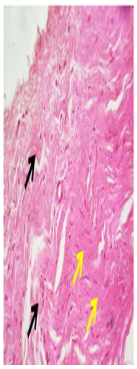

I. G1 Day 60: Histological section of the Achilles tendon showing limited vascularity, low cell density, and thick fibrotic scarring (black arrows). The thick but asymmetrically arranged collagen fibers showed poor alignment and little similarity to the typical tendon structure (yellow arrows). H&E stain, 40X.

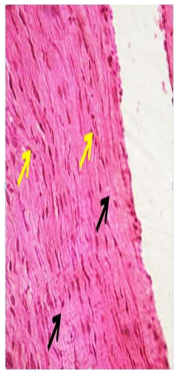

J. G2 Day 60: Histological section of the Achilles tendon showing dense collagen fiber deposition (black arrows). Fibroblasts were well organized with increased density (yellow arrows). H&E stain, 40X.

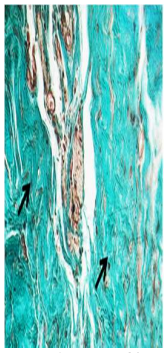

K. G1 Day 60: Masson trichrome-stained section showing dense, mostly green collagen fibers (black arrows), but they were not parallelly aligned and were irregularly organized. The tissue showed signs of fibrous scar formation, including disturbed architecture and lack of similarity to typical tendon structure. Masson trichrome stain, 40X.

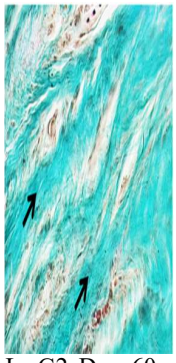

L. G2 Day 60: Masson trichrome-stained section showing more prevalent and better arranged collagen fibers compared with G1. Although some variation remained, the green-stained collagen bundles were partially aligned along the longitudinal direction of the tendon. Masson trichrome stain, 40X.

Discssion

As shown in the present study, it was found that the produced nanocellulose from the date palm tree (Phoenix dactylifera) via low-energy pulsed laser technique could enhance the healing process of the Achilles tendon when compared with the control group. According to FESEM analysis, it was found that the material had attained the nanoscale; however, FTIR, XRD, and UV-Vis analysis revealed that the material has kept its lignocellulosic functional groups and semicrystalline structures. The above findings are in line with those by Trache et al. [7] and Raza et al. [8], in which it was mentioned that the reduction of the size of cellulose to the nanoscale improves its surface area and biocompatibility without compromising its fundamental structural properties.

The physical effect of the use of low energy pulsed laser in the present study may be considered as facilitation by physical means leading to particles dispersion and to reduction of aggregation in the liquid medium and may not be considered as the physical agent which has triggered the formation of the nanostructures. According to Li et al. [24] the low power lasers may be used for the preparation of Cu_2O–Cu nanocomposites and the properties of nanoparticles prepared are determined by the energy of the laser beam and external conditions. In their study, Khraibet and Abdul Wahab [25] showed that the creation of silver nanoparticles using a low-power laser beam in conjunction with a natural plant extract could be beneficial, as confirmed by UV-Vis, FTIR, XRD, and FE-SEM research.

The present preparation technique is also in agreement with the observations made by Mamonova et al. [26] and Koo et al. [27] concerning the possibility of creating nanoparticles or their deposition using low-intensity or low-power lasers due to the local photochemical and thermal effects. This phenomenon was reported by Vinod et al. as well. [28] The nanoparticles can be prepared in water using low-energy laser pulses. In this way, the

results obtained during nanoscale tests in the present investigation can be explained in such a way that the low-energy laser is responsible for the miniaturization and dispersion processes, while *Albizia lebbeck* extract and DNA were responsible for the particle encapsulation and stabilization. Hence, the present approach is the example of laser-assisted green physical preparation.

On the other hand, the nanocellulose group showed rapid resolution of claudication, edema, erythema, and pain, together with better wound healing and decreased adhesions, in comparison to the control group. The other hand, the control group showed a persistent presence of inflammatory markers as well as a delayed repair of the wound, suggesting that this may have been the cause of the lack of biological support, as the wound was simply mended. This is consistent with the results obtained by Lin and Dufresne [23] and Ghilan et al. [22]. Nancellulose is a substance that promotes cell attachment and a regulation of the extracellular matrix, and is biocompatible. It shows good agreement with Schulze-Tanzil [29] and Andarawis-Puri et al. [30]. The authors showed that in order to heal a tendon, it must pass through a sequence of events, from inflammation to activation of the fibroblasts, to collagen deposition and remodelling. As such, the clinical effect the nanocellulose group is related to the improvement of tendon healing process itself.

This effect could be explained based on the fact that the use of nanocellulose provided a surface for easy migration and collagen deposition in the repair zone by fibroblasts that are biocompatible with a moist environment. Furthermore, the stabilization and improved local biocompatibility of the material might have been achieved since it was employed the extract of Albizia lebbeck which contains plant molecules and hydrolyzed polysaccharides with natural stabilizer. This is in agreement with the results obtained with the use of natural stabilizer by Balkrishna et al. [9] Kumar Varma and Jayaram Kumar [10]. Moreover, phenols have a potential to affect inflammation and oxidative stress mechanisms in the same manner as it was proposed by Yahfoufi et al. [31]. Therefore, it can be concluded here that nanocellulose could not only be used as a filler, but also provide a better local environment for fibroblasts and collagen formation. These results are confirmed by the ultrasound and histopathological findings. The control group maintained their heterogeneity and disorganized collagen fibers, whereas the nanocellulose group demonstrated more evident signs of changes in echogenicity, continuity of the tendons, less inflammatory infiltration, and improvement in organization of collagen fibers. Heterogeneous image in the control group is explained by the fact that tendon healing is a relatively slow process without a pro-inflammatory biomaterial. The presence of inflammation and disorganization of collagen fibers results in immature scar tissue that has more tendency to form adhesions. The results are in accordance with those of Buschmann et al. [32] who found that the improvement in image was caused by collagen maturation. They are also in agreement with Nichols et al. [33]. Provenzano and Vanderby [34] stated that the regeneration of function in tendons is mainly connected with regularity and orientation of collagen fibers rather than just the number of them. It is confirmed by the reviews made by Sharma and Maffulli [35] and Docheva et al. [36]. Mechanically, the benefit of the nanocellulose group to the control group at the time of the experiment seems to be ascribed to the greater organization of the collagen fibers and less level of inflammation in the local area. This is because the mechanical strength of the repaired tendon is not only related to the quality of the surgical closure of the gap but also to the quality of the tissue being produced by the wound and the maturity and direction of the collagen. Hence the slight less efficiency of the control group is attributed to the healing rather than the elimination of inflammation by the traditional surgery.

Conclusion

The study revealed that the use of nanocellulose obtained by the low level pulsed laser

technology from palm rachis in the treatment of Achilles tendon in rabbits was beneficial compared to the control group. This led to less inflammatory parameters in post surgery, improved healing and continuity of tendon fibres with increased echogenicity on ultrasound. Histological results revealed enhanced activity of fibroblasts, the regularity and deposition of collagen fibres and the mechanical strength of the tendon during healing. Hence, nanocellulose derived from palm frond has the potential to become a biocompatible biomaterial, locally available, that supports tendon regeneration and enhances the healing process.

Author Declarations

Conflict of Interest: No conflicts of interest.

Figures and Tables: All photos and data were generated by the authors and are not under permissions.Animal Experiments:All procedures were performed on adult New Zealand White rabbits in compliance with the institutional rules and all efforts were made to minimise pain and suffering.Ethical Considerations:The authors followed the ethical guidelines for research on animals.

Authors' Consent: All authors approved the final version of the paper and agreed to submit for publication.

References

1. Snedeker JG, Foolen J. Tendon injury and repair: a perspective on the basic mechanisms of tendon disease and future clinical therapy. *Acta Biomater.* 2017;63:18–36. doi:10.1016/j.actbio.2017.08.032.
2. Hammerman M, Pierantoni M, Isaksson H, Eliasson P. Deprivation of loading during rat Achilles tendon healing affects extracellular matrix composition and structure, and reduces cell density and alignment. *Sci Rep.* 2024;14(1):23380. doi:10.1038/s41598-024-74783-w.
3. Dobaj Štiglic A, Lackner F, Nagaraj C, Beaumont M, Bračič M, Duarte I, et al. 3D-printed collagen–nanocellulose hybrid bioscaffolds with tailored properties for tissue engineering applications. *ACS Appl Bio Mater.* 2023;6(12):5596–5608. doi:10.1021/acsabm.3c00767.
4. Galiwango E, Abdel Rahman NS, Al-Marzouqi AH, Abu-Omar MM, Khaleel AA. Isolation and characterization of cellulose and α-cellulose from date palm biomass waste. *Heliyon.* 2019;5(12):e02937. doi:10.1016/j.heliyon.2019.e02937.
5. Teo HL, Wahab RA. Towards an eco-friendly deconstruction of agro-industrial biomass and preparation of renewable cellulose nanomaterials: a review. *Int J Biol Macromol.* 2020;161:1414–1430. doi:10.1016/j.ijbiomac.2020.08.076.
6. Zahid I, Nazir MH, Javed MA. Extraction of bioactive components from date palm waste, various extraction processes and their applications: a review. *Biomass Bioenergy.* 2024;190:107433. doi:10.1016/j.biombioe.2024.107433.
7. Trache D, Tarchoun AF, Derradji M, Hamidon TS, Masruchin N, Brosse N, et al. Nanocellulose: from fundamentals to advanced applications. *Front Chem.* 2020;8:392. doi:10.3389/fchem.2020.00392.
8. Raza M, Abu-Jdayil B, Banat F, Al-Marzouqi AH. Isolation and characterization of cellulose nanocrystals from date palm waste. *ACS Omega.* 2022;7(29):25366–25379. doi:10.1021/acsomega.2c02333.
9. Balkrishna A, Sakshi, Chauhan M, Dabas A, Arya V. A comprehensive insight into the phytochemical, pharmacological potential, and traditional medicinal uses of *Albizia lebbeck* (L.) Benth. *Evid Based Complement Alternat Med.* 2022;2022:5359669. doi:10.1155/2022/5359669.
10. Kumar Varma CA, Jayaram Kumar K. Structural, functional and pH-sensitive release characteristics of water-soluble polysaccharide from the seeds of *Albizia lebbeck* L. *Carbohydr*

Polym. 2017;175:502–508. doi:10.1016/j.carbpol.2017.08.017.

11. Desjardins P, Conklin D. NanoDrop microvolume quantitation of nucleic acids. *J Vis Exp.* 2010;(45):e2565. doi:10.3791/2565.
12. Lee PY, Costumbrado J, Hsu CY, Kim YH. Agarose gel electrophoresis for the separation of DNA fragments. *J Vis Exp.* 2012;(62):e3923. doi:10.3791/3923.
13. Mangalam AP, Simonsen J, Benight AS. Cellulose/DNA hybrid nanomaterials. *Biomacromolecules.* 2009;10(3):497–504. doi:10.1021/bm800925x.
14. Bukharina D, Cauffiel K, Killingsworth LM, Brackenridge JA, Poliukhova V, Kim M, et al. Click-chemistry-enabled functionalization of cellulose nanocrystals with single-stranded DNA for directed assembly. *ACS Biomater Sci Eng.* 2024;10(10):6155–6166. doi:10.1021/acsbiomaterials.4c01518.
15. Yang X, Liang X, Nandi R, Tian Y, Zhang Y, Li Y, et al. DNA-modified liquid crystal droplets. Biosensors (Basel). 2022;12(5):275. doi:10.3390/bios12050275.
16. Fang C, Schmidt JE, Cybulska I, Brudecki GP, Frankær CG, Thomsen MH. Hydrothermal pretreatment of date palm (*Phoenix dactylifera* L.) leaflets and rachis to enhance enzymatic digestibility and bioethanol potential. *Biomed Res Int.* 2015;2015:216454. doi:10.1155/2015/216454.
17. Amendola V, Meneghetti M. Laser ablation synthesis in solution and size manipulation of noble metal nanoparticles. *Phys Chem Chem Phys.* 2009;11(20):3805–3821. doi:10.1039/B900654K.
18. Firoozeh F, Neshan A, Khaledi A, Zibaei M, Amiri A, Sobhani A, et al. Evaluation of the effect of magnetic nanoparticles on extraction of genomic DNA of *Escherichia coli*. *Polym Bull.* 2023;80(3):3153–3163. doi:10.1007/s00289-022-04196-0.
19. Hassan MA, Abdalla MA, Saber MS, Ali WS, Nassif M, Elsherif MW. Evaluation of xylazine-ketamine anesthesia in rabbits undergoing tendon surgery: a prospective randomized controlled study. *New Valley Vet J.* 2024;4(1):1–7. doi:10.21608/nvvj.2023.247402.1038.
20. Öztürk FA, Demirdöver C, Hüsemoğlu RB, Çakmak S, Ulukaya HE, Atalmış SE. A new 4-strand tendon repair technique in a rabbit Achilles tendon model: is 4 better than 6? *Acta Orthop Traumatol Turc.* 2023;57(2):67–72. doi:10.5152/j.aott.2023.22013.
21. Meier Bürgisser G, Calcagni M, Bachmann E, Fessel G, Snedeker JG, Giovanoli P, et al. Rabbit Achilles tendon full transection model: wound healing, adhesion formation and biomechanics at 3, 6 and 12 weeks post-surgery. *Biol Open.* 2016;5(9):1324–1333. doi:10.1242/bio.020644.
22. Ghilan A, Nicu R, Ciolacu DE, Ciolacu F. Insight into the latest medical applications of nanocellulose. Materials (Basel). 2023;16(12):4447. doi:10.3390/ma16124447.
23. Lin N, Dufresne A. Nanocellulose in biomedicine: current status and future prospect. *Eur Polym J.* 2014;59:302–325. doi:10.1016/j.eurpolymj.2014.07.025.
24. Li S, Lin Q, Liu X, Yang L, Ding J, Dong F, et al. Fast photocatalytic degradation of dyes using low-power laser-fabricated Cu_2O–Cu nanocomposites. RSC Adv. 2018;8:20277–20286. doi:10.1039/C8RA03117G.
25. Khraibet AA, Abdul Wahab AW. Green synthesis of silver nanoparticles using lemon juice extract assisted by low laser irradiation. Ann Chim Sci Mater. 2025;49(3):307–314. doi:10.18280/acsm.490307.
26. Mamonova DV, Petrov MI, Chernyak SA, et al. Laser-induced deposition of plasmonic Ag and Pt nanoparticles and periodic arrays. Materials. 2021;14(1):10. doi:10.3390/ma14010010.
27. Koo S, Park J, Kim J, et al. Green synthesis of nanoparticles using bio-inspired systems: laser-induced silver nanoparticle formation and

patterning. Nanomaterials. 2022;12(3):545. doi:10.3390/nano12030545.

28. Vinod M, Gopchandran KG, Unnikrishnan NV, et al. Ag@Au core-shell nanoparticles synthesized by pulsed laser ablation in water using low energy laser pulses. Spectrochim Acta A Mol Biomol Spectrosc. 2015;149:357–365. doi:10.1016/j.saa.2015.04.088
29. Schulze-Tanzil G. Healing of ligaments and tendons: tissue engineering and models. *Int J Mol Sci.* 2022;23(24):15503. doi:10.3390/ijms232415503.
30. Andarawis-Puri N, Flatow EL, Soslowsky LJ. Tendon basic science: development, repair, regeneration, and healing. *J Orthop Res*. 2015;33(6):780-784. doi:10.1002/jor.22869.
31. Yahfoufi N, Alsadi N, Jambi M, Matar C. The immunomodulatory and anti-inflammatory role of polyphenols. *Nutrients*. 2018;10(11):1618. doi:10.3390/nu10111618.
32. Buschmann J, Puippe G, Meier Bürgisser G, Bonavoglia E, Giovanoli P, Calcagni M. Correspondence of high-frequency ultrasound and histomorphometry of healing rabbit Achilles tendon tissue. *Connect Tissue Res.* 2014;55(2):123–131. doi:10.3109/03008207.2013.870162.
33. Nichols AEC, Best KT, Loiselle AE. The cellular basis of fibrotic tendon healing: challenges and opportunities. *Transl Res.* 2019;209:156–168. doi:10.1016/j.trsl.2019.02.002.
34. Provenzano PP, Vanderby R Jr. Collagen fibril morphology and organization: implications for force transmission in ligament and tendon. *Matrix Biol.* 2006;25(2):71–84. doi:10.1016/j.matbio.2005.09.005.
35. Sharma P, Maffulli N. Tendon injury and tendinopathy: healing and repair. *J Bone Joint Surg Am*. 2005;87(1):187-202. doi:10.2106/JBJS.D.01850.
36. Docheva D, Müller SA, Majewski M, Evans CH. Biologics for tendon repair. *Adv Drug Deliv Rev*. 2015;84:222-239. doi:10.1016/j.addr.2014.11.015.
37. Zhu S, He Z, Ji L, Zhang W, Tong Y, Luo J, et al. Advanced nanofiber-based scaffolds for Achilles tendon regenerative engineering. Front Bioeng Biotechnol. 2022;10:897010. doi:10.3389/fbioe.2022.897010.
38. Iravani S. Green synthesis of metal nanoparticles using plants. *Green Chem.* 2011;13(10):2638–2650. doi:10.1039/C1GC15386B.
39. Kuşcu B, Bilal Ö, Doğar F, Topak D, Gürbüz K, Dere Kİ, et al. Effects of L-carnitine on healing of Achilles tendon in rats. *Jt Dis Relat Surg.* 2023;34(1):84–91. doi:10.52312/jdrs.2023.853.